



Microchannel with Waviness at Selective Locations for Liquid Cooling of Microelectromechanical Devices

D. Sathish Kumar and S. Jayavel[†]

Department of Mechanical Engineering, Indian Institute of Information Technology Design and Manufacturing Kancheepuram, Chennai - 600127, India

[†]Corresponding Author Email: sjv@iiitdm.ac.in

(Received May 30, 2020; accepted November 17, 2020)

ABSTRACT

Miniaturized electronic components require effective heat transfer mechanism to dissipate heat with less surface area available for convective heat dissipation. Liquid cooling system with in-built microchannel is one of the feasible options. The new idea proposed in the present work is incorporation of waviness at selective locations in the microchannel. This method enhances heat transfer as well as maintains uniform surface temperature. Three-dimensional numerical simulations are carried out using ANSYS Fluent 15. Water is taken as the working fluid. Present numerical results of base case with plane wall are validated using published experimental and numerical results available in literature. Systematic study has been conducted by varying the flow Reynolds number and design parameters *viz.*, wave amplitude and wavelength of the waviness on bottom wall. The computational results are presented in the form of Nusselt number, pressure drop and friction factor. Performance of the wavy wall microchannel is better with short wavelengths. In the present configuration of rectangular microchannel, wave amplitude of $0.2D_h$ with wavelength of $3D_h$ shows optimum performance. Moreover, selective waviness on bottom wall shows better performance with uniform surface temperature.

Keywords: Liquid cooling; Microchannel; Local waviness; Heat transfer enhancement.

NOMENCLATURE

A	amplitude	q	heat flux
a	channel dimension	Re	Reynolds number
AR	aspect ratio	Re_c	critical Reynolds number
C_p	specific heat	V_{ch}	flow velocity in the channel
D_h	hydraulic diameter	W_{ch}	channel width
f	fanning friction factor	x	coordinate axis in the flow direction
H_{ch}	channel height	y	coordinate axis in the transverse direction
h	heat transfer coefficient	μ	dynamic viscosity
h_{avg}	average heat transfer coefficient	ΔP	channel pressure drop
k_f	fluid thermal conductivity	ν	kinematic viscosity
L_{ch}	channel length	ρ	density
L_e	entry length	Ω	pumping power
Nu	Nusselt number	λ	wavelength
P	pressure		
P_{wet}	wetted perimeter		

1. INTRODUCTION

Engineering systems such as mechanical, electrical, electronic, etc. undergo processes with net result being the generation of heat. Increase in temperature due to heat generation has adverse effect on reliability and performance of the system.

Electronic industries are migrating towards miniaturization of components, but with increased performance. The twofold development leads to more heat generation with less surface area available for heat dissipation. Complexity of thermal management is therefore increased and technology advancement is required. Liquid flow

Table 1a Classification of channels

S. No	Reference	Nano channels	Micro channels	Mini channels	Conventional channels
1	Kandilakar <i>et al.</i> (2005)	$0.1\mu\text{m} \geq D$	$200\mu\text{m} \geq D > 10\mu\text{m}$	$3\text{mm} \geq D > 200\mu\text{m}$	$> 3\text{mm}$
2	Mehendale <i>et al.</i> (2000)	-	$100\mu\text{m} \geq D > 1\mu\text{m}$		$> 6\text{mm}$
3	Celata <i>et al.</i> (2004)	-	$1\text{mm} \geq D > 1\mu\text{m}$	-	-
4	Gad-el-Hak (2005)	-	$1\text{mm} \geq D > 1\mu\text{m}$	-	$> 1\text{mm}$
5	Peng <i>et al.</i> (1994)	-	$1\text{mm} \geq D > 100\mu\text{m}$	-	-
6	Garimella <i>et al.</i> (2004)	-	$0.97\text{mm} \geq D > 244\mu\text{m}$	-	-
7	Kharati-Koopaei <i>et al.</i> (2018)	-	$D = 1\text{ mm}$	-	-

Table 1b Classification of channels

S. No	Reference	Transitional nano channels	Transitional micro channels	Meso channels	Compact passages
1	Kandilakar <i>et al.</i> (2005)	$1\mu\text{m} \geq D > 0.1\mu\text{m}$	$10\mu\text{m} \geq D > 1\mu\text{m}$	-	-
2	Mehendale <i>et al.</i> (2000)	-	-	$1\text{mm} \geq D > 100\mu\text{m}$	$6\text{mm} \geq D > 1\text{mm}$

through microchannel is one of the compact and efficient cooling systems. Classification of microchannels is elaborated by Kandilkar *et al.* (2005). Further, Celata *et al.* (2004) and Peng *et al.* (1994) have also carried out heat transfer study in narrow channels and designated as nano / micro / mini channels based on the hydraulic diameter. Based on channel dimension, the classification of narrow channels as proposed by various researchers is presented in Table – 1. From the comparison, the channel hydraulic diameter in the range of $1\text{mm} \geq D_h > 1\mu\text{m}$ is considered to be microchannel in the present study, experimental investigation on microchannel for laminar flow ($\text{Re} \leq 2100$) in confined channels conducted by Tuckerman and Pease (1981) showed increase in heat transfer with decreasing channel width and decrease in thermal resistance with increasing aspect ratio. Total thermal resistance in the liquid cooling system as defined by Tuckerman and Pease (1981) is the sum of three components *viz.*, (i) resistance due to conduction from circuits through substrate and heat-sink interface, (ii) resistance due to convection from heat sink to the cooling liquid and (iii) resistance due to heating of the fluid. The authors studied the effect of channel width varying from 0.05 to 0.056 mm and channel height varying from 0.28 to 0.32 mm. They suggested to locate the sink near heat source to reduce resistance. The authors have also suggested to increase the flow rate and to select fluid with high heat capacity to reduce heating resistance. Hydraulic diameter is one of the geometry parameters that affects friction factor in rectangular microchannels. Peng *et al.* (1994) conducted experiments to study the effect of hydraulic diameter varying from 0.113 to 0.367 mm for various flow velocities in the range 0.25 to 12 m/s ($50 \leq \text{Re} \leq 4000$) and reported transition in microchannel at $\text{Re} < 1000$. The critical Re was

found to increase from 200 to 700 for hydraulic diameter in the range 0.133 to 0.367 mm. However, Sahar *et al.* (2016), Zhang *et al.* (2014) and Pfund *et al.* (2000) did not observe early transition. Mokrani *et al.* (2009) experimentally investigated the fluid flow and convective heat transfer in rectangular microchannels by varying the channel height ($0.05 \leq H_{ch} \leq 0.5\text{mm}$) and kept the width as constant. For $D_h > 1$, the correlations for normal channel were found to be applicable. However, $H_{ch} < 0.05$ mm, the results are found to deviate from the conventional correlations. The authors validated their results using the conventional relations available in Shah and London (1978) and found that the results match well. Sahar *et al.* (2016) assumed thin wall with zero wall thickness for two-dimensional computations, whereas conjugate heat transfer analysis was carried out for 3D multichannel domain. Two different configurations were simulated, (i) single channel with hydraulic diameter of 0.561 mm and (ii) multichannel (25 channels with $D_h = 0.409$ mm) consisting of inlets and outlets connected to manifolds.

The two-dimensional numerical results of Sahar *et al.* (2016) under-predicted friction factor values by about 30%. The results obtained from three-dimensional study are found to match well with the experimental data. This shows the presence of three-dimensional effect in the flow. Pfund *et al.* (2000) conducted experimental investigation in the range $0.0128 \leq AR \leq 0.105$ and $0.025 \leq D_h \leq 0.19$ mm and the transition was observed in the range, $1500 \leq \text{Re} \leq 2200$. Their results showed deviation of the non-dimensional Poiseuille number (product of friction factor and Re) from the correlations proposed by Shah and London (1978). The reason for the deviation might be due to experimental uncertainties. Wang *et al.* (2016) conducted

numerical analysis on rectangular, trapezoidal and triangular shaped microchannel heat sinks with varying hydraulic diameter and aspect ratio. The influence of geometric parameters of microchannel on flow and heat transfer was significant. The microchannel with high aspect ratio, large wetted perimeter and small hydraulic diameters showed low thermal resistance and high pressure drop. Thermal resistance for triangular and trapezoidal heat sinks was respectively, 11.82% and 1.01% higher than that of rectangular heat sink. [Amirah et al. \(2017\)](#) reported increase in average Nu with hydraulic diameter. Therefore, it is interesting to explore the effect of microchannel geometry on heat transfer.

Increase in surface area enhances heat transfer in microchannels with minimum increase in pressure drop. [Sui et al. \(2010\)](#) conducted numerical analysis of three-dimensional wavy microchannels with rectangular cross section and mentioned the advantage of providing waviness in the channel wall. The location and magnitude of vortices along the flow direction varies with respect to wave amplitude and wavelength. Numerical simulations with constant wall-heat-flux and constant wall-temperature boundary conditions for Re in the range, 100 to 800 were conducted. It was found that increasing the wave amplitude along the direction of flow leads to better thermal performance. Three-dimensional experimental and numerical study was conducted for half-corrugated microchannels by [Wan et al. \(2017\)](#) and the results were compared with flat bottom microchannels to analyze the pressure drop and thermal performance. Based on the hydro-thermal performance index values, it was recommended that half-corrugated microchannels are better than double sinusoidal corrugated channels. For low Re values, it was noted that the effect of wave amplitude on pressure drop is insignificant, whereas the wavelength effect is more dominant. [Rostami et al. \(2015\)](#) and [Gong et al. \(2011\)](#) have studied the effects of various parameters such as, aspect ratio, wavelength and amplitude and reported improved performance. [Wang et al. \(2002\)](#) and [Lin et al. \(2017\)](#) have also reported significant improvement in heat transfer performance due to wavy wall. [Wang et al. \(2002\)](#) used a factor defined as the ratio between amplitude and wavelength of the waviness and observed better performance with higher values of the ratio. [Ghani et al. \(2017\)](#) conducted study on channel with sinusoidal cavities and rectangular ribs. The comparative analysis was conducted between the channels with rectangular ribs, channel with sinusoidal cavities and channel with both sinusoidal cavities and rectangular ribs. The performance of microchannel with sinusoidal cavities and rectangular ribs was found to have significant improvement in performance at high Re compared to the other two configurations. [Duangthongsuk and Wongwises \(2017\)](#) introduced zig-zag flow to increase the heat transfer area. With different volume fractions of nanofluid, the crosscut zig-zag channel showed better thermal performance.

Geometry and surface modification are the two major components that significantly affect the performance of microchannel. Geometry of the microchannel includes dimensions, shape and cross-section of the channel. On the other hand, surface modification includes incorporation of wall waviness, fins, ribs, cavities, coils, tapes, etc. The objectives of the modifications are maximum enhancement in heat transfer with minimum increase in pressure drop. In the present study, waviness on channel wall has been incorporated at selective location to disturb thermal boundary layer, to increase available convective surface area and to enhance mixing. The waviness at selective location meets both the objectives of maximum heat transfer enhancement and minimum increase in pressure drop.

2. PROBLEM DESCRIPTION AND SOLUTION METHODOLOGY

Flow and heat transfer characteristics in microchannel with wall waviness at selective locations as shown in Fig.1 are studied. The equation used to define the sinusoidal wave is given in Eq. (10). The study has been carried out for rectangular cross-sectional channels with fixed $AR = 1$ and $D_h = 1\text{mm}$. Length of the channel is 62mm. The waviness is provided for the length of 42 mm in the downstream of the channel and the first 20mm of channel length is kept as plane i.e. without waviness. The present study is conducted by varying the wavelength ($3D_h \leq \lambda \leq 12D_h$) of the wavy wall. The effect of amplitude ($0.1D_h \leq A \leq 3D_h$) on the flow and thermal characteristics are also studied for various Reynolds number. The heat transfer enhancement has been compared with the plane geometry. To validate the present numerical results, rectangular microchannel with dimensions, $W_{ch} \times H_{ch} \times L_{ch}$ is considered, where $W_{ch} \times H_{ch}$ is the flow cross-section and L_{ch} is the length of the microchannel. For validation purpose the confining walls are considered plane as shown in Fig. 2 and constant heat flux is applied. The computational domain consists of two cylindrical plenums of diameter 2 mm and height 8 mm as shown in Fig. 2(a). To validate the present methodology, the domain and the geometry are same as the one studied by [Amirah et al. \(2017\)](#). Working fluid is water and the inlet temperature is 27°C. The corresponding fluid properties are given in Table 2. Fluid enters through one of the plenums and comes out from the other. Microchannel of 62mm length connects the two plenums as shown in Fig. 2(a). Three-dimensional numerical study has been carried out with constant aspect ratio ($AR = 1$). Hydraulic diameter (D_h) is varied from 0.1 mm to 1 mm. Further, the effect of Re ($300 \leq Re \leq 1500$) has been studied. As reported in literature ([Liu et al. 2004](#), [Pfund et al. 2000](#) and [Gao et al. 2002](#)), flow in the microchannel is considered as laminar for $Re \leq 1500$.

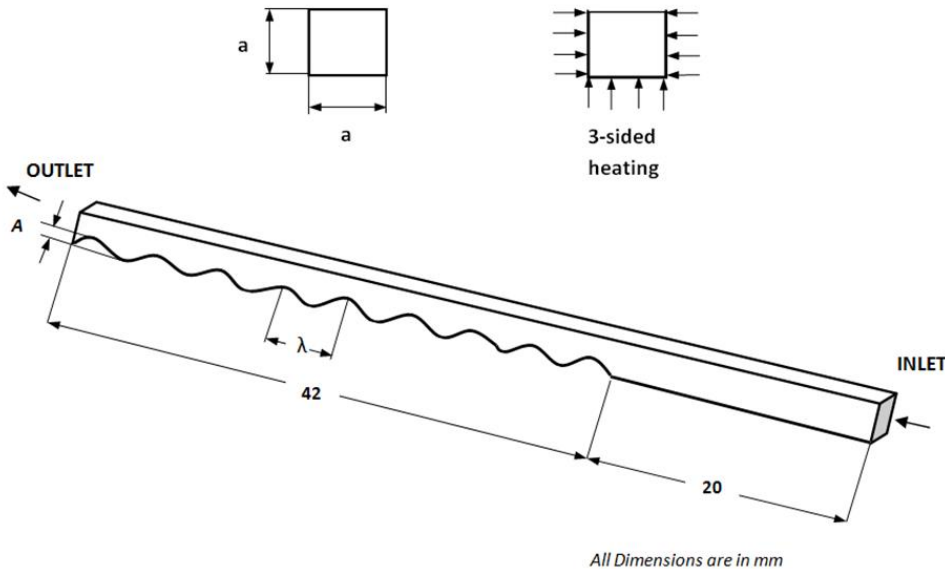


Fig. 1. Schematic representation of the computational domain with waviness at selective location in the channel.

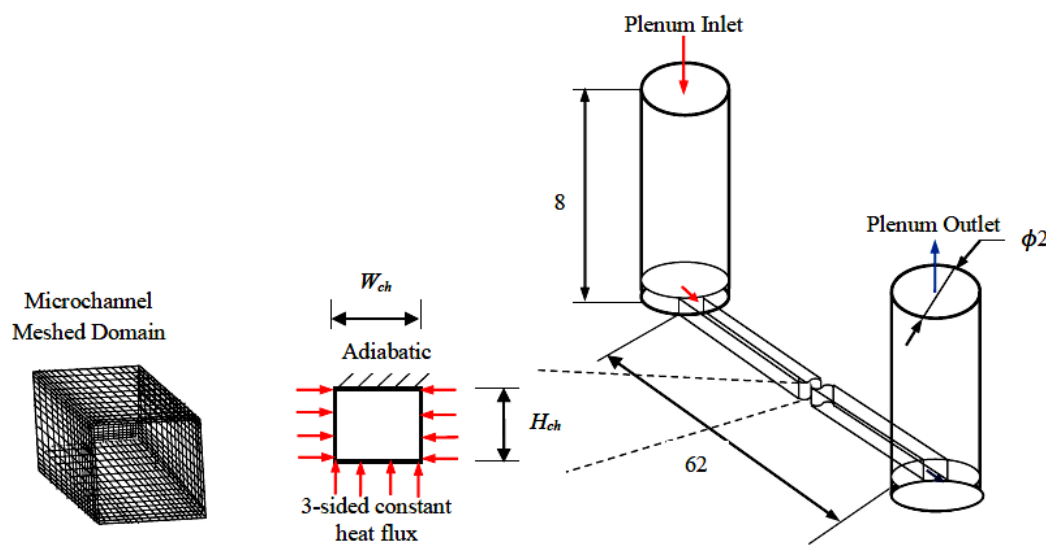


Fig. 2. Computational domain schematic representation (b) meshed domain.

Table 2 Properties of working fluid at 27°C

Properties	Water
Density (kg/m^3)	996.5
Kinematic viscosity (m^2/s)	0.853×10^{-6}
Thermal conductivity (W/mK)	0.6
Specific heat (kJ/kgK)	4.181
Prandtl number	5.5

The meshed domain is shown in Fig. 2(b). ICEM CFD is used for grid generation. Boundary conditions imposed are: uniform velocity at the plenum inlet and zero static pressure at outlet of the other plenum. Constant heat-flux value of 150

kW/m^2 is applied at three (bottom and both vertical) walls. The top wall is considered to be adiabatic. The summary of boundary conditions is given in Table 3. The governing equations applicable to the present study are given in Eqs. (1) to (3). Further, the assumptions imposed are incompressible, laminar, steady flow with constant fluid property and negligible radiation heat transfer. ANSYS Fluent Version 15 is used for simulations with a convergence criterion of 10^{-6} . Both momentum and energy equations are solved using first order upwind scheme. SIMPLE scheme is used to solve pressure-velocity coupling. Optimum grid size has been chosen by conducting grid independence study. The flow and heat transfer parameters used in

the present study are given in Eqs. (4) to (8).

$$\nabla \cdot \vec{V} = 0 \quad (1)$$

$$\rho (\vec{V} \cdot \nabla \vec{V}) = -\nabla p + \nabla \cdot (\mu \nabla \vec{V}) \quad (2)$$

$$\rho c_p (\vec{V} \cdot \nabla T) = k \nabla^2 T \quad (3)$$

$$Re = \frac{\rho V_{ch} D_h}{\mu} \quad (4)$$

$$AR = \frac{H_{ch}}{W_{ch}} \quad (5)$$

$$D_h = \frac{4A}{P} = \frac{4(H_{ch} W_{ch})}{2(H_{ch} + W_{ch})} \quad (6)$$

$$f = \frac{\Delta P D_{ch}}{2L_{ch} \rho V_{ch}^2}; \quad \Delta P = P_{ch,in} - P_{ch,out} \quad (7)$$

$$Nu = \frac{h D_h}{k}; \quad h = \frac{q}{T_{wall,avg} - T_{fluid,avg}} \quad (8)$$

$$\Omega = \dot{Q} \Delta P \quad (9)$$

Table 3 Summary of boundary conditions

Boundary	Condition
Inlet	$u = u_{in}, v = 0, w = 0$
Outlet	$\frac{\partial p}{\partial x} = 0$
Top and side walls	$u = 0, v = 0, w = 0$
Bottom wall	$u = 0, v = 0, w = 0,$ $q = 150 kW / m^2 (const)$

where, Q is volumetric flow rate,

$$Q = Re \nu a$$

The following equation is used to define the sinusoidal waviness on the bottom wall

$$y = A \sin\left(\frac{2\pi x}{\lambda}\right) \quad (10)$$

3. RESULTS AND DISCUSSIONS

This section presents the simulated results, which includes grid independence study, validation of the present results and detailed discussion on thermo-fluid characteristics due to waviness on bottom wall at selective locations.

Table 4 Grid independence study

Grid size ($H_{ch} \times W_{ch} \times L_{ch}$)	Nu _{avg}	% Deviation
12 12 200	7.0123	--
13×13×250	7.1235	1.585
15×15×200	7.1928	0.979
15×15×300	7.1906	0.03

3.1 Grid Independence Study

Grid independence study has been carried out to identify optimum grid size so as to obtain results with good accuracy in minimum possible computational time. Nu_{avg} is used as the parameter to check grid independence. The geometry and flow parameters used for the study are $D_h = 1$ mm, $AR = 1$, and $Re = 500$. The variation in Nu_{avg} with respect to grid size is presented in Table 4. Mesh with 15×15×200 nodes has been identified as the optimum grid size and used for further computations.

3.2 Validation of Computed Results

To verify the present computational methodology and to obtain accurate results, a thorough validation check has been conducted using the results available in literature ([Amirah et al. 2017](#), [Sahar et al. 2016](#) and [Shah and London 1978](#)).

Table 5 Deviation of friction factor values with Amirah et al. (2017)

D_h (mm)	Amirah et al. (2017) (Re = 500)	Present Study (Re = 500)	% Deviation
0.1	0.031	0.028	9.6
0.5	0.033	0.031	6
1	0.039	0.034	12.8

Table 6 Pressure drop (AR=1)

D_h (mm)	Re	ΔP , (Pa)		Deviation (%)
		Present study	Amirah et al. (2017)	
0.1	586	553300	528469	4.4
0.5	537	4704	4523.58	3.8
1	585	812.1	766.77	5.5

Table 7 Hydrodynamic entry length (in meters)

Re	Present Study	Galvis et al. (2012)	% Deviation
300	0.0128	0.0135	5.18
500	0.021	0.022	4
700	0.0304	0.031	1.9

3.2.1 Effect of Hydraulic Diameter on Friction Factor

The friction factor for various D_h ($D_h = 0.1, 0.5, 1$ mm) and $AR = 1$ are computed for the range of Re , $100 \leq Re \leq 1500$. The results are shown in Fig. 3. The friction factor values are calculated using Eq. (7). Present results match well with [Amirah et al. \(2017\)](#) at high Re . At low Re , around 10% deviation is found. The reason for the deviation may be due to ignoring minor losses at entry and exit of channel in the present study. For the sake of understanding, the values for $Re = 500$ are presented in Table-5. In order to validate the present numerical results with

experimental results of [Sahar et al. \(2016\)](#), a hydraulic diameter of 0.56 mm has been taken for simulation and the friction factor values are found to match very well with the results available in the

literature.

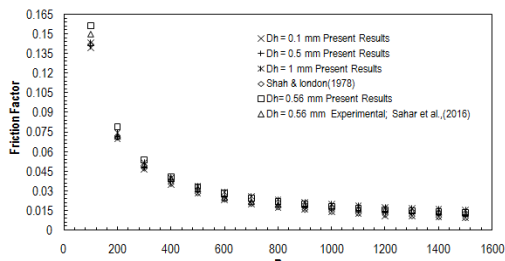


Fig. 3. Effect of hydraulic diameter on friction factor.

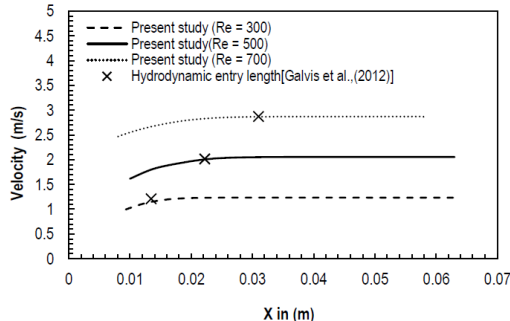


Fig. 4. Centre-line velocity variation along the flow direction for $D_h = 0.5$ mm and $AR = 1$.

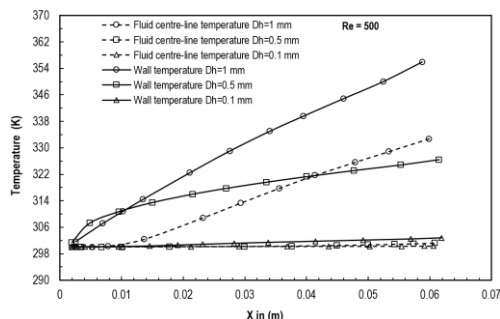


Fig. 5. Temperature variation along flow direction ($Re = 500$).

3.2.2 Pressure Drop

Pressure drop is calculated as the difference in pressures between the inlet and outlet of the channel. The total pressure drop is the pressure difference from inlet to outlet of the plenum. The channel pressure drop without considering the minor losses is used for calculating the friction factor. Validation of the present results is given in Table 6. The deviation increases with hydraulic diameter, D_h . Sudden change in pressure is observed due to the 90° change in flow direction at plenum-channel intersections *i.e.*, at channel inlet and outlet. Amirah *et al.* (2017), calculated pressure drop by considering entry and exit losses. The entry losses is in the range 2.37% to 14.19% and the exit losses are in the range 1.36% to 29.67% for $D_h = 0.1$ to 1 mm.

3.2.3 Hydrodynamic Entry Length

The velocity variation along the channel length for $Re = 300, 500$ and 700 with $D_h = 0.5$ mm is shown in Fig. 4. The curves in the figure are showing the

centre-line along the channel to know where exactly the flow is fully developed. At $Re = 500$, hydrodynamic entry length is observed as 21 mm from inlet of the channel and the value is compared with the correlation (Eq. 11) available in literature (Galvis *et al.* 2012) and the values are found matching. The results are presented in Table 7.

$$\frac{L_e}{D_h} = \frac{0.740}{0.09R_e + 1} + 0.0889R_e \quad (11)$$

3.2.4 Temperature Variation along the Channel Length

The effect of D_h on heat transfer for $Re = 500$ has been studied and the temperature variation along the channel for various D_h is shown in the Fig. 5. The wall temperatures at inlet and outlet are 28°C and 54°C , respectively. Whereas, from inlet to exit, the fluid temperature rise is from 27°C to 29°C . These temperature differences are for $D_h = 0.5$ mm.

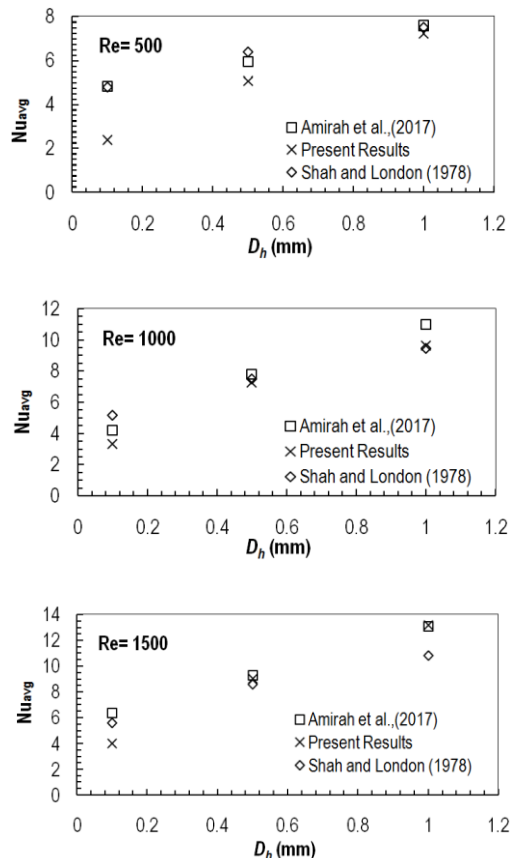


Fig. 6. Effect of D_h on average Nusselt number ($AR = 1$).

Along the flow direction the difference in temperature between the channel wall and fluid centerline increase. Relatively more temperature difference in downstream indicates relatively less heat transfer in the downstream. Therefore, in the present study, waviness on the bottom wall is incorporated at selective downstream region to enhance heat transfer.

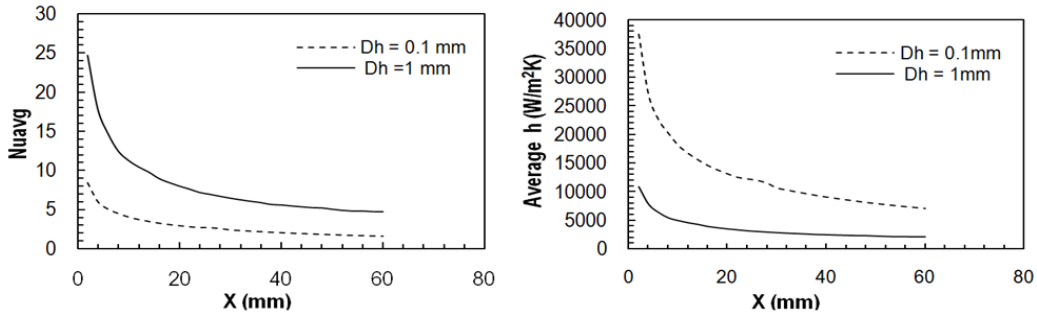


Fig. 7. Variation of Nusselt number and heat transfer coefficient (without waviness) $Re = 500$ and $AR=1$.

Table 8 Specifications of computed rectangular microchannels ($AR = 1, D_h = 1\text{mm}$)

Channel Geometry	Test Case	Wavelength (λ) D_h	Amplitude (A) D_h
1	Plane Channel (PC)	∞	0
2	Wavy Channel (WC-1)	3	0.2
3	Wavy Channel (WC-2)	6	0.2
4	Wavy Channel (WC-3)	9	0.2
5	Wavy Channel (WC-4)	12	0.2
6	Wavy Channel (WC-5)	6	0.1
7	Wavy Channel (WC-6)	6	0.15
8	Wavy Channel (WC-7)	6	0.25
9	Wavy Channel (WC-8)	6	0.3

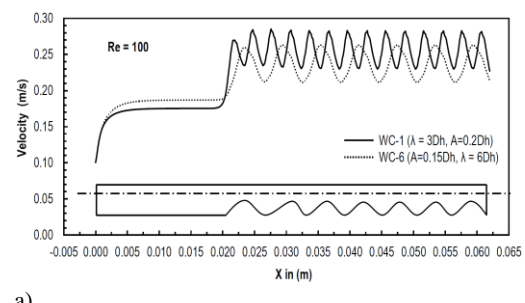
3.2.5 Effect of Hydraulic Diameter on Heat Transfer

Nu variation with D_h in the range $0.1 \leq D_h \leq 1 \text{ mm}$ has been studied. The average Nu increases with D_h . The present results are compared with numerical results of [Amirah et al. \(2017\)](#) and [Shah and London \(1978\)](#) as shown in Fig. 6. The variation of average Nu and average heat transfer coefficient along the channel axis for $D_h = 0.1$ and 1 mm are shown in Fig.7. The value of the heat transfer coefficient for $D_h = 0.1 \text{ mm}$ is higher compared to $D_h = 1 \text{ mm}$. Although, Nu is directly proportional to hydraulic diameter and heat transfer coefficient ($\text{Nu} = hD_h/k$), the results show that with increasing D_h , Nu increases, but heat transfer coefficient decreases. This is because for the given thermal conductivity, D_h is more dominant compared to heat transfer coefficient. From this analysis, the significance of geometry parameter D_h on heat transfer is observed.

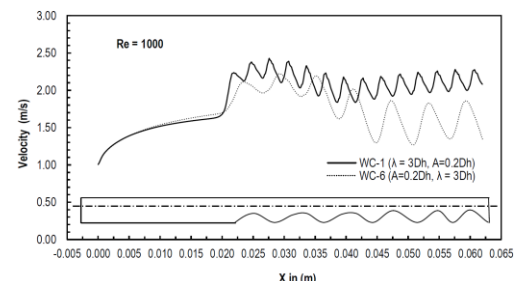
3.3 Waviness on Bottom Wall

Main aim of the present study is to enhance thermal performance of microchannel by surface modification *i.e.* providing waviness on the bottom wall. The waviness enhances mixing in the highly confined flow through straight microchannel. Previous studies *viz.*, [Lin et al. \(2017\)](#) and [Wan et al. \(2017\)](#) are dealt with waviness and corrugation on full length of the channel sidewall. It is observed from the present and previous results that the average value of axial Nu and h decreases along the

flow direction irrespective of the channel D_h . As shown in Fig. 7, the decrease in the values is observed up to a distance of 20mm from the channel inlet. The same trend is noticed in both minimum and maximum value of channel D_h .



a)



b)

Fig. 8. Velocity variation along channel length for WC-1, 6 at (a) $Re = 100$; (b) $Re = 1000$.

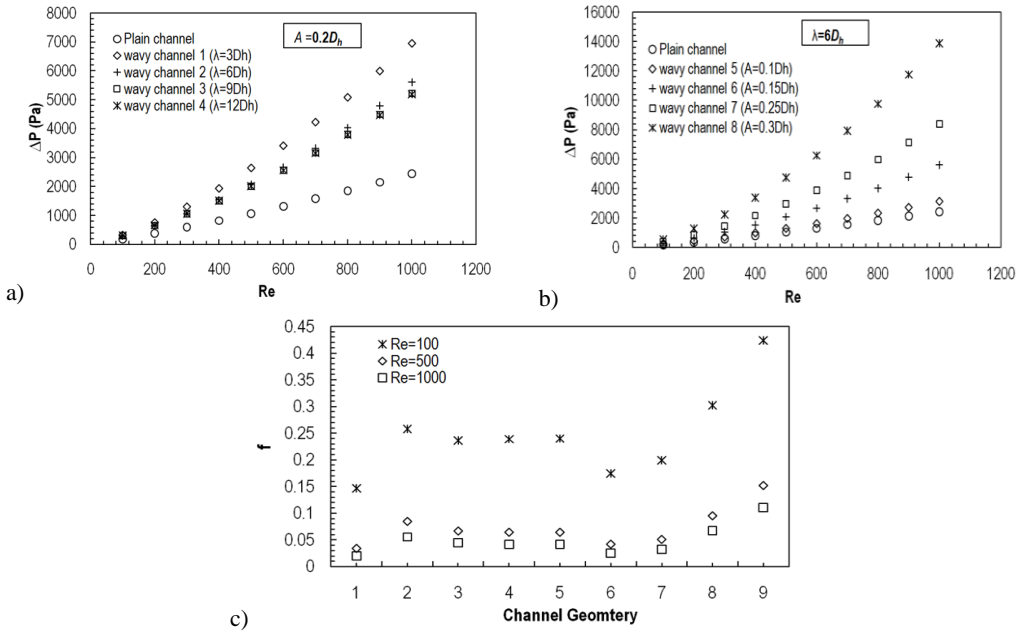


Fig. 9. Variation of pressure drop and friction factor (a) effect of Re on pressure drop for fixed A (b) effect of Re on pressure drop for fixed λ (c) effect of channel geometry on friction factor.

Therefore, heat transfer enhancement is required at the downstream rather than full length of the channel wall. Therefore, in the present study, 20mm from the channel inlet is unaltered. Waviness is incorporated at bottom wall in the downstream. Numerical analysis has been carried out for a wide range of wavelength and amplitude. Flow rate of working fluid varied from 0.0000001 to 0.000001 m³/s and the various cases considered in the present study are listed in Table - 8. The simulated results are compared with simple plane (smooth wall) rectangular microchannel ($AR = 1$ and $D_h = 1$ mm).

3.3.1 Effect of Bottom Wall Waviness on Flow Characteristics

Velocity fluctuations along the centerline due to the presence of crest and trough in wavy channels are shown in Fig. 8. At low Re, ($Re = 100$) the maximum and minimum values of the fluctuating velocity are found repeating until the channel outlet. However, irregular fluctuations are observed at higher Re. When the flow is at higher Re, the fluid molecules in trough region is dragged by the fluid which is flowing near to crest region and molecules with higher velocity will support the motion of the molecule with lower velocity. This might be the reason for fluctuation in centreline velocity. But this behaviour doesn't happen when the flow is at low speed. The effects of Re and wavelength on pressure drop are shown in Fig. 9(a) for fixed wave amplitude ($A = 0.2D_h$). The total pressure drop is calculated using Eqn. (12) (Wan *et al.* 2017). The first term in right side of Eq. (12) represents the friction between fluid layers and with the channel wall. The second term accounts the pressure drop due to wavy geometry. The increase in pressure drop is almost linear with Re and the trend is

looking similar for all wavelengths considered. At low Re, ($Re \leq 200$) the effect of wavelength on ΔP is negligible and the wavelength effect is observed from $Re = 200$ to 1000. This shows that for a given A , the wavy bottom performs better at low Re for a wide range of λ . As Re increases, the increase in ΔP is significant for shorter wavelength. Waviness with larger λ leads to orderly flow and reduces ΔP .

$$\Delta P = \Delta P_f + n\Delta P_r \quad (12)$$

Figure 9 (b) shows the effect of wave amplitude on ΔP for various Re. Amplitude, A is varied from

$0.1D_h$ to $3D_h$ and λ is fixed ($\lambda = 6D_h$). Increase in wave amplitude increases ΔP . The increase in pressure drop with amplitude is more dominant with increasing Re. Friction factor values of both plane and wavy channels for lower, medium and larger Re values are shown in Fig. 9(c). The contour plot (Fig.10a) shows the effect of λ and A on pressure drop at $Re = 100$ and 1000.

The microchannel with $A = 0.3D_h$ and $\lambda = 6D_h$ (WC-8) produces maximum pressure drop. For $A > 0.25D_h$, large pressure drop is observed with λ in the range, $5D_h \leq \lambda \leq 8D_h$. The ΔP in plane (PC) and wavy (WC-1 to 8) channels for low, medium and high Re values are shown in Fig.10 (b) and (c). At $Re = 100$, the values are almost same for all the cases considered. The ΔP values decrease for channel geometries *i.e.*, WC-1 to 5 (varying λ with constant A) as shown in Fig. 10(b). However, the ΔP values increases for the remaining channel geometries *i.e.*, WC-5 to 8 (varying A with constant λ). An undesirable phenomenon of very high ΔP is observed for channel geometries WC-7 to 8 due to high amplitude of the wavy wall. Among all wavy wall channel geometries, WC-5 ($\lambda=6D_h$, $A = 0.1D_h$)

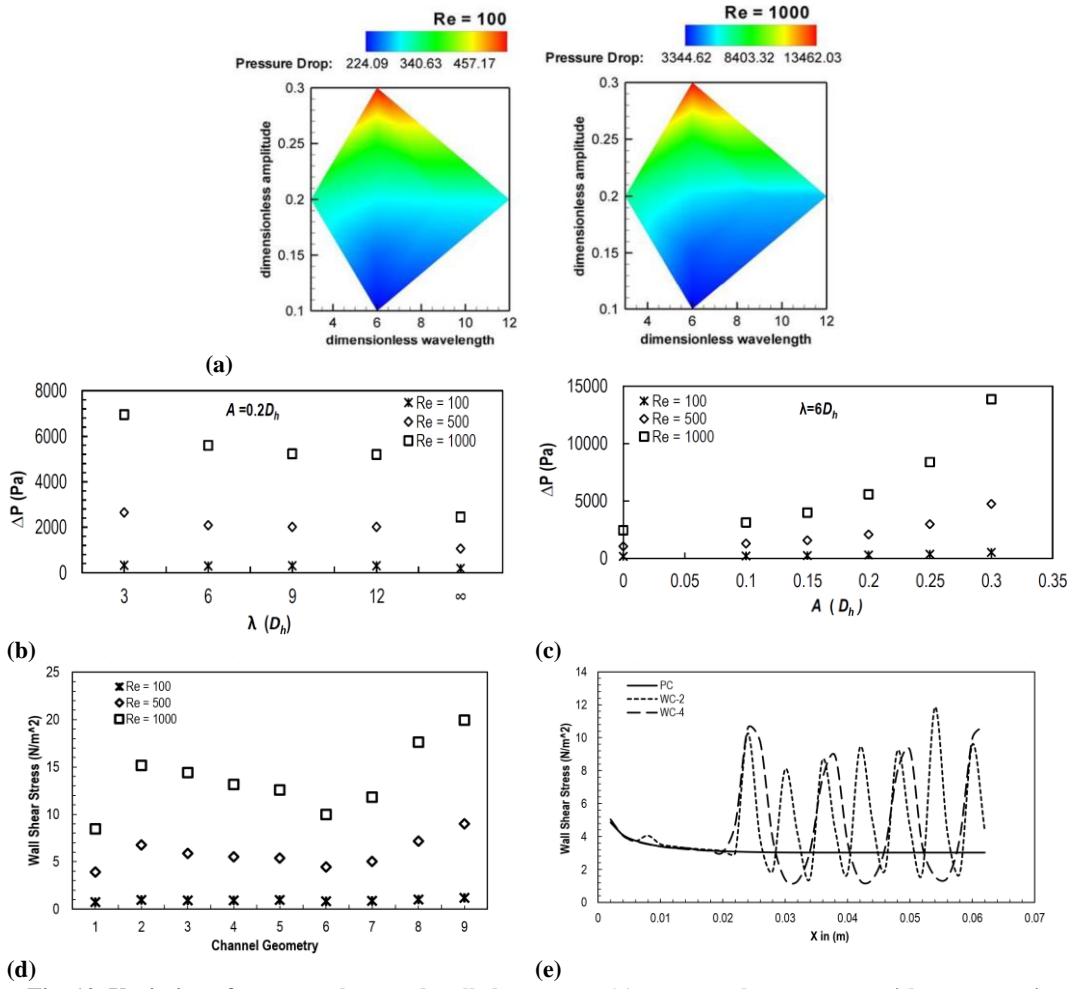


Fig. 10. Variation of pressure drop and wall shear stress (a) pressure drop contour with respect to λ and A (b) effect of λ on pressure drop (c) effect of A on pressure drop (d) effect of channel geometry wall shear stress (e) axial wall shear stress comparison

Table 9 Friction factor and wall shear stress variation among all geometries (Re=500)

Channel Geometry	$\lambda (D_h)$	$A (D_h)$	Pressure drop (Pa)	Friction factor	Wall shear stress(N/m^2)
PC	∞	0	1060.0	0.0339	3.92
WC-1	3	0.2	2645.1	0.0846	6.58
WC-2	6	0.2	2080.7	0.0665	5.73
WC-3	9	0.2	2010.3	0.0643	5.46
WC-4	12	0.2	2007.5	0.0642	5.38
WC-5	6	0.1	1306.3	0.0418	4.43
WC-6	6	0.15	1586.6	0.0507	4.93
WC-7	6	0.25	2977.2	0.0952	6.99
WC-8	6	0.3	4758.8	0.1523	9.01

shows lowest ΔP , even at high Re values. Friction factor and wall shear stress variation are calculated and presented in Table-7 for $Re = 500$. The increase in form drag due to increase in amplitude of the waviness is clearly observed from the results as presented in Table-9. The increase in form drag is more dominant at higher Re . The fluctuating wall shear stress is observed only in wavy channels, while the shear stress in plane channel decreases linearly along the flow direction as shown in Fig. 10(d) and Fig. 10(e).

3.3.2 Effect of Bottom Wall Waviness on Heat Transfer

In the microchannel heat sink with plane wall channel, the thick boundary layer leads to poor heat transfer. In the present study, the boundary layer in the downstream is disturbed by providing waviness on the bottom wall. The presence of waviness in the bottom wall may cause recirculation and secondary flows in the channel vortices. Figure 11(a) shows the effect of waviness on Nu for a wide range of Re .

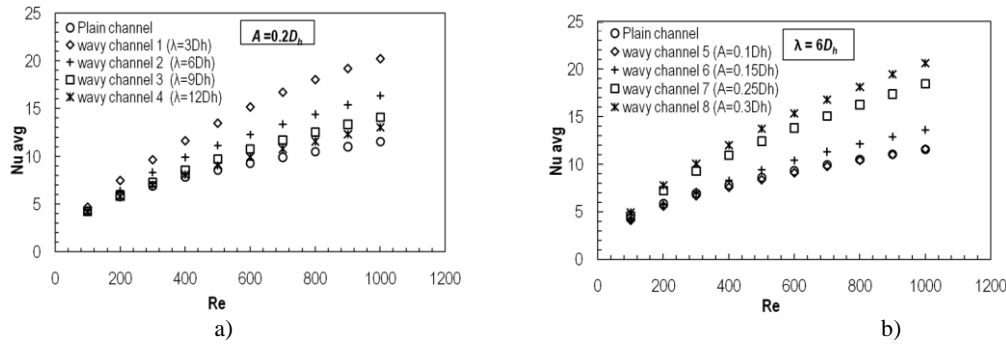


Fig. 11. Effect of Re on average Nu for both wavy and plane microchannels (a) for various λ ; (b) for various A .

The results are compared with plane wall. As expected, the Nu increases as the flow rate increases for all cases irrespective of the type of wall. At any particular value of Re, a smaller value of wavelength disturbs the boundary layer in a better way and results in higher Nu. As wavelength of wavy wall increases, the boundary layer is less affected and there is no significant increase in Nu. The influence of waviness on Nu at low Re (Re <200) is negligible. At higher Reynolds number, the presence of waviness leads to considerable increase in heat transfer enhancement. At Re = 1000, for WC-1, the Nu is 20.24. This value is 1.75 times greater than that of the plane channel. Simulations are carried out by varying the amplitude, A and keeping λ constant and the results are shown in Fig. 11(b). As expected, wherever pressure drop is high, Nu is also showing an enhancement. For higher Re, WC-7 and WC-8 are showing better performance than WC-5 and WC-6, because of higher A . The heat transfer enhancement is supported by two factors; one is incremental surface area and second by disturbing the boundary layer. Our study is mainly focussed on heat transfer enhancement by disturbing boundary layer than by increasing the surface area. The surface area values are given in Fig. 16. In WC-5, due to small value of wave amplitude, the heat transfer enhancement is not supported much by disturbing boundary layer. Meanwhile, the surface area of WC-5 is less compared with Plane channel. This might be the reason for lower Nu values when compared with Plane channel.

Based on the obtained numerical results the following relation (Eqn.13) is found for Nusselt number. The correlation is the function of Re, wavelength (λ) and wave amplitude (A). The numerical results match with proposed correlation for wavy channel as shown in Fig.12.

$$Nu = \left\{ \left[\frac{-0.6049}{10000} Re^2 \right] + \left[\frac{16.5157}{100} Re \right] + [2.5238 Re^{0.1} K^{-0.41}] - [11.8276] \right\} \times \left\{ K^{0.41} \right\}$$

Where,

$$K = \left\{ \frac{A^{2.1452}}{\lambda} \right\} \quad (13)$$

The average Nu variation along the flow direction for both PC and WC are shown in Fig.13 for various Reynolds number. The variation is smooth up to the channel length of 20 mm from the inlet. Fluctuation starts in the downstream of channel where waviness is incorporated. WC-2, which has shorter wavelength, produces more peaks in Nu values along the flow direction. From practical point of view, non-uniform temperature distribution on the surface is a common problem in miniaturized electronic components. With this novel idea of incorporating waviness at selective locations provides localized heat transfer enhancement and thereby eliminates hot spots in practical applications.

The effect of A and λ on heat transfer are studied and Nu variation with respect to A and λ are shown in Fig. 14(a). At Re = 100, for $A \leq 0.2D_h$ the effect of λ is not significant but, for the same Re the maximum value of average Nu is found with WC-8 ($\lambda=6D_h$ and $A=0.3D_h$). The heat transfer coefficient and Nu values are more at higher Re as expected. Figure 14(b) shows the thermal performance of all wavy wall channels (WC-1 to 8) and compared with PC. At higher Re the influence is more significant. At any particular Re, the values for WC-5 is less compared to WC-8, because recirculation of fluid occurs near upper portion of wavy region. This recirculation disturbs the boundary layer and enhances mixing of the near wall fluid with the main stream fluid in WC-8 configuration.

3.4 Performance Analysis

Hydro-thermal performance as defined in Eq. (14) is a measure of performance index (PI) accounting

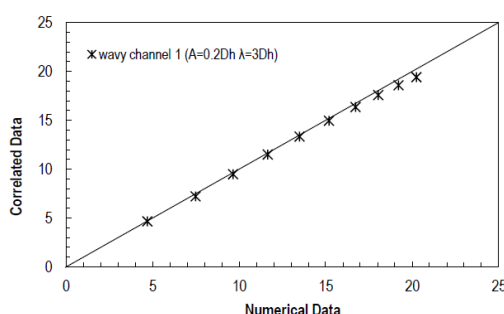


Fig. 12. Comparison of numerical results with proposed correlation for all computed Re.

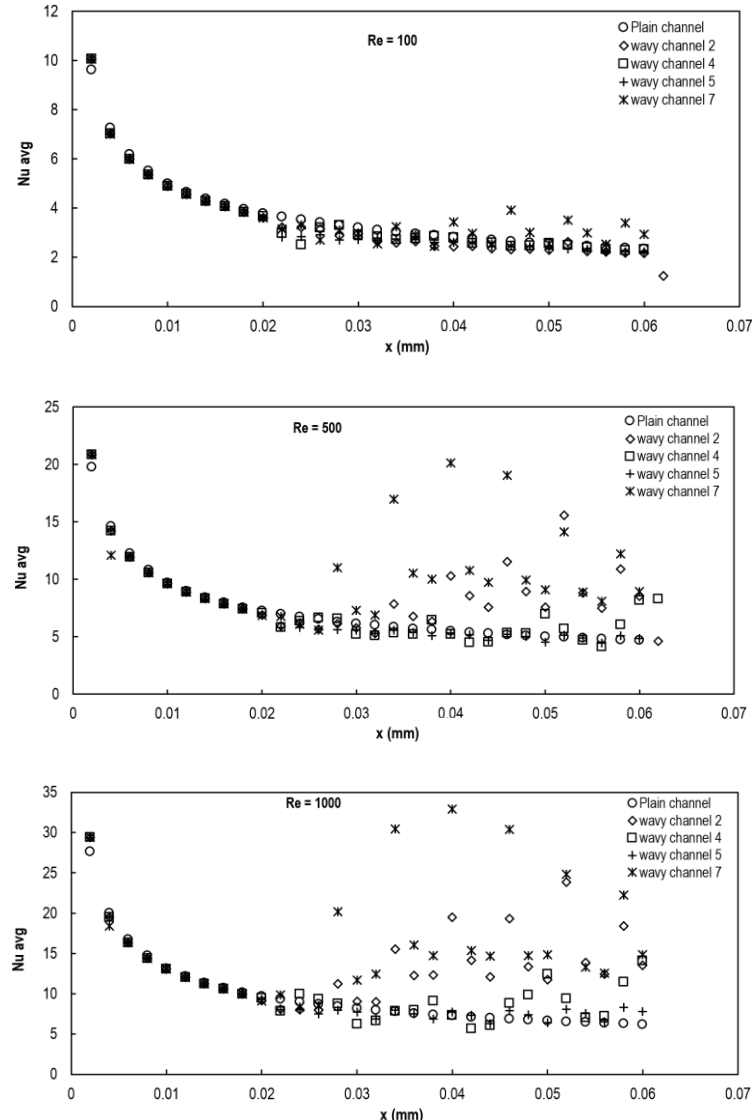


Fig. 13. Axial Nusselt number variation in plane channel (PC) and channel with wavy wall (WC-2,4,5,7).

for heat transfer enhancement with associated pressure drop, where the subscript (o) refers to plane wall microchannel. PI > 1 indicates better hydro-thermal performance.

$$PI = \frac{Nu/Nu_0}{\left(\frac{f/f_0}{\lambda}\right)^{\frac{1}{3}}} \quad (14)$$

The overall PI values for different channel geometries and the significance of λ and A are shown in Fig. 15. In general, microchannel with wavy wall is superior than plane channel for all computed Re values. This indicates achievement of heat transfer enhancement with minimum increase in pressure drop. The maximum value of PI is at WC-1 ($A = 0.2D_h$ and $\lambda = 3D_h$). If wavelength increases (from WC-2 to 4) the PI value decreases for fixed value of A . But there is decreasing-increasing trend in PI values when A value increases with constant λ . This shows the influence of friction factor which also showed a irregular

pattern as shown in Fig. 9c. Moreover, for $A > 0.2D_h$ undesirable increase in pumping power is observed. The individual surface area and pumping power at Re = 500 is shown in Fig. 16. The pressure drop at WC-8 is very high than other wavy channels and corresponding pumping power is 5 times than plane (smooth wall) channel. The amplitude of WC-8 is very high among all other wavy channels and the fluid flow getting disturbed more when it passes through all wavy units because the passage between upper wall and crest portion of wavy units is very small. This was the reason for poor PI value for WC-8 and more pumping power.

4. CONCLUSIONS

Three-dimensional numerical study on flow and thermal characteristics for flow through microchannel with rectangular cross section has been carried out. The new design incorporates waviness on bottom wall of the microchannel at

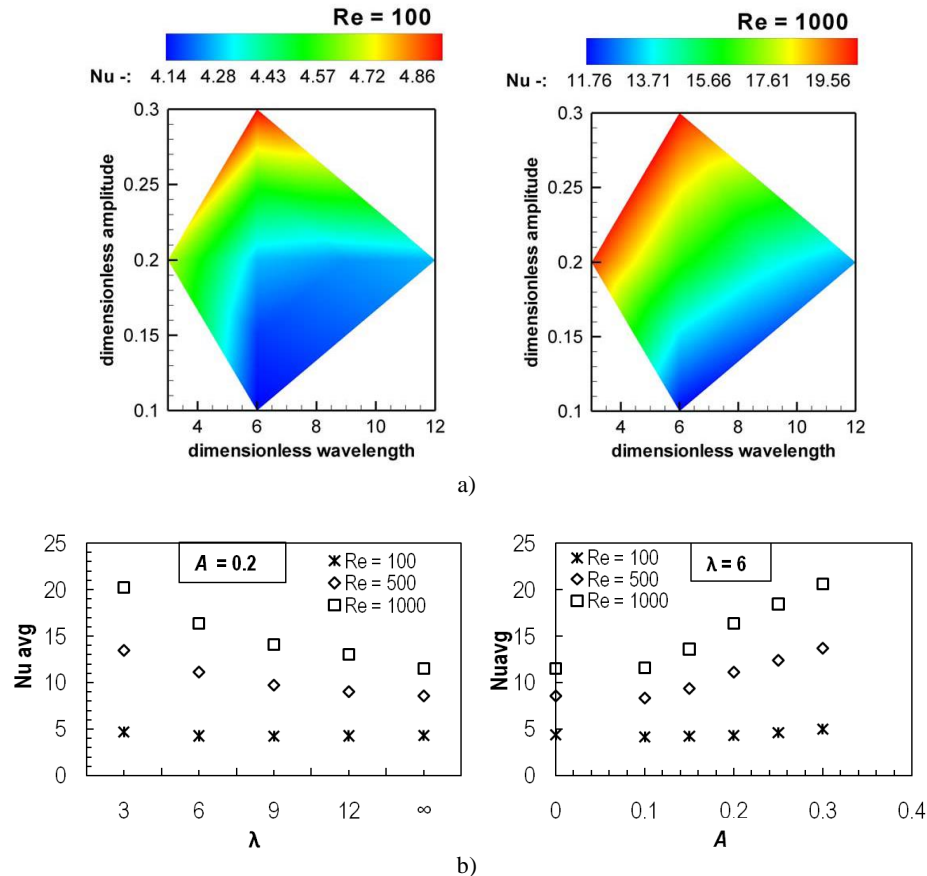


Fig. 14. (a) Nu contour with respect to λ and A (b)Effect of λ and A on Nu.

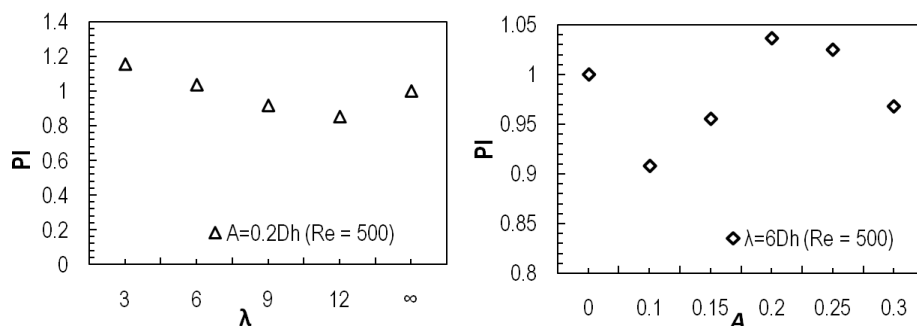


Fig. 15. Effect of λ and A on Performance index.

selective location. The effect of design parameters such as amplitude, A and wavelength, λ on the microchannel performance are presented for a wide range of Re. The observations from the simulation results are summarized below

1. Experimental and numerical results, available in literature are used for validation purpose. Thorough validation of the presents results are carried out.
2. The friction factor and averaged Nu is found to increase with hydraulic diameter of the microchannel. However, the effect of hydraulic diameter on hydrodynamic entry length is

insignificant.

3. Waviness at selective locations on the bottom wall of microchannel is found to enhance heat transfer. The wavelength, λ and amplitude, A of the waviness are the significant parameters that affect the performance. Maximum enhancement in Nu is 78.9% that is observed for the case, WC-8.
4. The increase in pressure drop with A is more dominant with increasing Re. The channel wall with ($A = 0.3D_h$) and ($\lambda = 6D_h$) (Case No.: WC-8) produces maximum pressure drop.

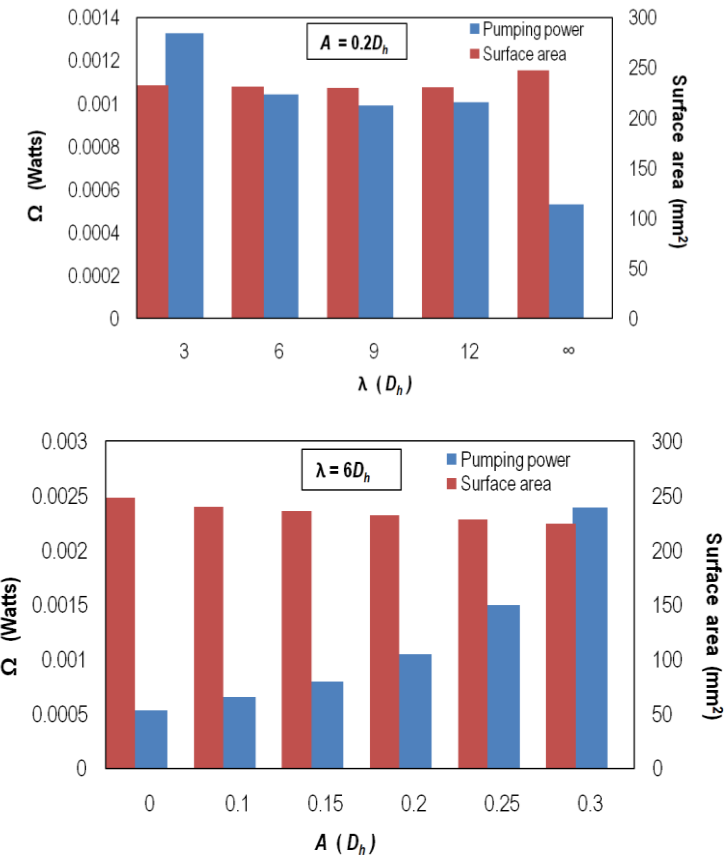


Fig. 16. Pumping power and surface area for plane and wavy channels. The performance of the proposed channel geometries (WC 1-8) are compared with plane channel.

5. Shorter the wavelength, better is its effect on boundary layer therefore better Nu. The influence of waviness on Nu at low Re ($Re < 200$) is negligible.
6. Introduction of local waviness in microchannels with appropriate amplitude and wavelengths eliminates hot spots and results in uniform surface temperature. At $Re = 100$, for $A \leq 0.2D_h$, the effect of λ is not significant and shows poor thermal performance. For the same Re, the maximum value of average Nu is found with WC-8 ($\lambda=6D_h$ and $A=0.3D_h$).
7. The maximum value of PI is for WC-1 ($A = 0.2D_h$ and $\lambda = 3D_h$). For a given wave amplitude, with increasing wavelength (from WC-2 to 4) the PI value decreases.

REFERENCES

- Amirah, M. Sahar, J. Wissink, M. M. Mahmoud, T. G. Karayannidis and M. S. A. Ishak (2017). Effect of hydraulic diameter and aspect ratio on single phase flow and heat transfer in a rectangular microchannel. *Applied Thermal Engineering* 115, 793-814.
- Celata, G. P. (2004) *Heat transfer and fluid flow in microchannels*, Begell House Inc., NY.
- Duangthongsuk, W. and S. Wongwises (2017). An experimental investigation on the heat transfer and pressure drop characteristics of nanofluid flowing in microchannel heat sink with multiple zigzag flow channel structures. *Experimental Thermal and Fluid Science* 87, 30-39.
- Gad-el-Hak, M. (Ed.) (2005). MEMS: Introduction and Fundamentals. CRC press.
- Galvis, E., S. Yarusevych and J. R. Culham (2012). Incompressible laminar developing flow in microchannels. *Journal of Fluid Engineering* 134(1).
- Gao, P., S. Le Person, and M. Favre-Marinet (2002). Scale effects on hydrodynamics and heat transfer in two-dimensional mini and microchannels. *International Journal of Thermal Sciences* 41(11), 1017-1027.
- Garimella, S. V. and V. Singhal (2004). Single-phase flow and heat transport and pumping considerations in microchannel heat sinks. *Heat Transfer Engineering* 25(1), 15-25.
- Ghani, I. A., N. Kamaruzaman and N. A. C. Sidik (2017). Heat transfer augmentation in a microchannel heat sink with sinusoidal cavities and rectangular ribs. *International Journal of Heat and Mass Transfer* 108, 1969-1981.
- Gong, L., K. Kota, W. Tao and Y. Joshi (2011).

- Parametric numerical study of flow and heat transfer in microchannels with wavy walls. *ASME Journal of Heat Transfer* 133(5). 051702.
- Kandlikar, S., S. Garimella, D. Li, S. Colin and M. R. King (2005). *Heat transfer and fluid flow in minichannels and microchannels*. Elsevier.
- Kharati-Koopaei, M. and M. R. Akhtari (2018). Numerical study of fluid flow and heat transfer phenomenon within microchannels comprising different superhydrophobic structures. *International Journal of Thermal Sciences* 124, 536-546.
- Lin, L., J. Zhao, G. Lu, X. D. Wang and W. M. Yan (2017). Heat transfer enhancement in microchannel heat sink by wavy channel with changing wavelength/amplitude. *International Journal of Thermal Sciences* 118, 423-434.
- Liu, D. and S. V. Garimella (2004). Investigation of liquid flow in microchannels. *Journal of Thermophysics and heat transfer* 18(1), 65-72.
- Mehendale, S. S., A. M. Jacobi and R. K. Shah (2000). Fluid flow and heat transfer at micro- and meso-scales with application to heat exchanger design. *ASME Applied Mechanics Reviews* 53(7), 175-193.
- Mokrani, O., B. Bourouga, C. Castelain and H. Peerhossaini (2009). Fluid flow and convective heat transfer in flat microchannels. *International Journal of Heat and Mass Transfer* 52(5-6), 1337-1352.
- Peng, X. F., G. P. Peterson and B. X. Wang (1994). Frictional flow characteristics of water flowing through rectangular microchannels. *Experimental Heat Transfer An International Journal* 7(4), 249-264.
- Pfund, D., D. Rector, A. Shekarriz, A. Popescu and J. Welty (2000). Pressure drop measurements in a microchannel. *AIChE Journal* 46(8), 1496-1507.
- Rostami, J., A. Abbassi and M. Saffar-Aval (2015). Optimization of conjugate heat transfer in wavy walls microchannels. *Applied Thermal Engineering* 82, 318-328.
- Sahar, A. M., M. R. Özdemir, E. M. Fayyadh, J. Wissink, M. M. Mahmoud and T. G. Karayannis (2016). Single phase flow pressure drop and heat transfer in rectangular metallic microchannels. *Applied Thermal Engineering* 93, 1324-1336.
- Shah, R. K. and A. London (1978) *Laminar flow forced convection in ducts*, in: T.F. Irvine, J. P. Hartnett (Eds.), *Advances in Heat Transfer* (Suppl. 1), Academic Press, New York.
- Sui, Y., C. J. Teo, P. S. Lee, Y. T. Chew and C. Shu (2010). Fluid flow and heat transfer in wavy microchannels. *International Journal of Heat and Mass Transfer* 53(13-14), 2760-2772.
- Tuckerman, D. B. and R. F. W. Pease (1981). High-performance heat sinking for VLSI. *IEEE Electron device letters* 2(5), 126-129.
- Wan, Z., Q. Lin, X. Wang and Y. Tang (2017). Flow characteristics and heat transfer performance of half-corrugated microchannels. *Applied Thermal Engineering* 123, 1140-1151.
- Wang, C. C. and C. K. Chen (2002). Forced convection in a wavy-wall channel. *International Journal of Heat and Mass Transfer* 45(12), 2587-2595.
- Wang, H., Z. Chen and J. Gao (2016). Influence of geometric parameters on flow and heat transfer performance of micro-channel heat sinks. *Applied Thermal Engineering* 107, 870-879.
- Zhang, J., Y. H. Diao, Y. H. Zhao and Y. N. Zhang (2014). An experimental study of the characteristics of fluid flow and heat transfer in the multiport microchannel flat tube. *Applied Thermal Engineering* 65(1-2), 209-218.